An enhanced terminal guidance law for short-range aerial vehicles with impact angle constraints and aerodynamic uncertainty

Pham Duc Thong[1*], D. V. Tarlakovsky[2]

[1]Institute of Missile, Academy of Military Science and Technology, 17 Hoang Sam, Nghia Do, Hanoi, Vietnam;
[2]Lomonosov Moscow State University, №1 Ulitsa Kolmogorova, Moscow, Russian Federation.
[*]Corresponding author: dtstudio.pro@gmail.com
Received 06 Jun. 2026; Revised 19 Aug. 2026; Accepted 04 Sep. 2026; Published 16 Sep. 2026.
DOI: https://doi.org/10.54939/1859-1043.j.mst.FMC.2026.133-141

ABSTRACT

In terminal guidance for short-range aerial vehicles, especially in scenarios involving attacks on maritime targets, ensuring the required approach angle is a decisive factor in mission effectiveness. The same vehicle can be significantly more effective when approaching the target at the correct angle than when merely reaching the correct position without satisfying the desired approach-angle condition. However, this requirement is difficult to fulfill in practice because of the combined effects of continuously varying sea-surface winds and aerodynamic uncertainties when the vehicle operates in low-dynamic-pressure conditions near the sea surface. This paper proposes a terminal guidance law for short-range aerial vehicles employing a skid-to-turn control configuration, in which the approach trajectory is regenerated at each guidance cycle in the form of a second- or third-order Bézier curve, while simultaneously satisfying both positional and angular constraints at the terminal point. Based on this reference trajectory, the required velocity-direction rates are transformed into commands for the angle of attack, α, and the sideslip angle, β, through a closed-form dynamic-inversion step. Monte Carlo simulation results obtained using the reference model show that the proposed method achieves a circular error probable of less than 1 m and a terminal flight-path-angle error of less than 1.5 degrees, while maintaining robustness against uncertainties in wind, atmospheric density, and aerodynamic coefficients.

Keywords: Aerodynamic uncertainty; Bezier curves; Impact angle; Onboard guidance; Terminal guidance; Trajectory regeneration.

1. INTRODUCTION

In many modern combat missions, aerial vehicles are required not only to strike the target accurately but also to approach it from a predetermined direction. The approach angle-defined as the angle between the velocity vector and the local horizontal plane at the moment of target engagement-is an important parameter because it directly affects mission effectiveness and the ability to maintain an approach trajectory outside the close-range defense zone [1, 2]. This requirement is particularly stringent for short-range aerial vehicles (SRAVs) operating over both sea and land [3, 4], especially in maritime attack scenarios where near-surface wind conditions vary continuously in both magnitude and direction. Under such conditions, maintaining an accurate approach angle becomes a central challenge, since the guidance law must simultaneously cope with fluctuating sea-surface winds and aerodynamic uncertainties when the vehicle operates in low-dynamic-pressure conditions near the sea surface [5].

At present, proportional navigation and its variants remain a common foundation for terminal-guidance problems [1], but they often require additional correction or adaptation terms to satisfy the approach-angle constraint [6]. Sliding-mode control laws [7, 8], integrated guidance and control schemes [9, 10], and optimization-based methods such as model predictive control [11, 12] have also demonstrated good performance. Another approach is to shape the trajectory using smooth parametric curves [13-15]. Among these, the Bézier curve is particularly attractive because

of its clear analytical form, its ability to conveniently impose boundary conditions, and its successful application in impact-time control, impact-angle control, Apollo–Bézier hybrid structures, and the interception of maneuvering targets [13-15]. However, most existing studies focus mainly on high-speed vehicles or bank-to-turn control configurations, whereas short-range aerial vehicles employing skid-to-turn (STT) control have received limited attention. This class of vehicles exhibits several distinctive characteristics, including short flight range, operation in dense atmospheric conditions, and control through the angle of attack, α, and the sideslip angle, β, rather than through the bank angle.

Unlike the methods in [13-15], this paper develops a Bézier-based guidance framework specifically for SRAVs with STT control. The main contributions are threefold: (1) the reference trajectory is replanned at each guidance cycle using the current estimated vehicle state, following a receding-horizon-like mechanism rather than relying on a fixed trajectory; (2) quadratic and cubic Bézier curves are selected according to the prescribed approach angle, providing flexible trajectory reconstruction from sea-skimming flight to steep terminal dives; and (3) a closed-form dynamic-inversion formulation directly generates the angle-of-attack and sideslip-angle commands, α_c and β_c, without requiring arctangent evaluation, matrix inversion, or iterative numerical procedures. Monte Carlo simulations demonstrate that the proposed method achieves a circular error probable (CEP) below 1 m and a terminal flight-path-angle error below 1.5°, while maintaining robust performance under uncertainties in wind, atmospheric density, and aerodynamic coefficients.

2. PROBLEM FORMULATION

2.1. Terminal engagement scenario

Consider an SRAV entering its terminal phase at time t_0, after completing the midcourse flight segment under inertial guidance combined with landmark-based correction. The terminal phase begins when the seeker acquires the target, typically at a range of 3–5 km for seekers of this class operating in the laser or infrared bands, and ends upon target impact. In the terminal-phase trajectory coordinate system, the origin is located at the target, and the aiming point is defined as $\left(L_f, 0, h_f\right)$. Guidance is considered successful if, at the final time T, the aerial vehicle approaches the target with sufficient positional accuracy and from the prescribed direction.

$$\mathrm{P}_{g(T)} = \mathrm{P}\left\{\begin{matrix}\left|L(T)-L_f\right| \le \varepsilon_L, \left|B(T)\right| \le \varepsilon_B, \left|h(T)-h_f\right| \le \varepsilon_h, \\ \Theta_{\min} \le \Theta(T) \le \Theta_{\max}, \Psi_{\min} \le \Psi(T) \le \Psi_{\max}\end{matrix}\right\} \ge \mathrm{P}_{req} \tag{1}$$

Here L, B, h are the longitudinal, lateral, and altitude coordinates; Θ and Ψ are the flight path and heading angles; $\varepsilon_L, \varepsilon_B, \varepsilon_h$ bound the admissible miss; $\left[\Theta_{\min}, \Theta_{\max}\right]$ and $\left[\Psi_{\min}, \Psi_{\max}\right]$ come from the required impact elevation δ_{inc} and azimuth Az_{inc}.

2.2. Flight dynamics

The equations of motion are formulated in the orbital coordinate system. For a terminal-phase problem spanning only a few kilometers, as considered in this study, the flat-Earth assumption is acceptable. Accordingly, terms associated with Earth curvature, as well as transport and Coriolis accelerations, are neglected. However, the translational equations of motion retain their full nonlinear form, including the coupling between the longitudinal and lateral channels induced by aerodynamic effects:

$$\dot{\Theta} = \frac{Y\cos\gamma - Z\sin\gamma}{mV} - \frac{g}{V}\cos\Theta, \qquad \dot{\Psi} = -\frac{Y\sin\gamma + Z\cos\gamma}{mV\cos\Theta} \tag{2}$$

with $\dot{h} = V\sin\Theta$, $\dot{L} = V\cos\Theta\cos\Psi$, and $\dot{B} = V\cos\Theta\sin\Psi$. The aerodynamic forces are $X = \frac{1}{2}\rho V^2 \cdot C_x$, $Y = \frac{1}{2}\rho V^2 S \cdot C_y$, $Z = \frac{1}{2}\rho V^2 S \cdot C_z$, with C_x, C_y, C_z depending on α, β, Mach number, and surface deflections. The state vector is $X = \left[h,\ L,\ B,\ V,\ \Theta,\ \Psi,\ \alpha,\ \beta\right]^T$.

2.3. STT angular loop

In the STT configuration, the bank angle is maintained approximately at zero ($\gamma \approx 0$), so changes in the direction of the velocity vector are generated mainly by two control channels: the angle of attack, α, and the sideslip angle, β. Based on this, the inner-loop control model is formulated as follows:

$$\frac{\alpha(s)}{\alpha_{com}(s)} = \frac{K_\alpha}{T_\alpha^2 s^2 + 2T_\alpha \xi_\alpha s + 1}, \quad \frac{\beta(s)}{\beta_{com}(s)} = \frac{K_\beta}{T_\beta^2 s^2 + 2T_\beta \xi_\beta s + 1}, \quad \gamma_{com} \equiv 0 \tag{3}$$

with a settling time $\tau \le 0.3$ s and damping ratio $\xi = 0.7$ for the SRAV class considered. Commands are hard-limited as $\alpha_{\min} \le \alpha_{com} \le \alpha_{\max}$ and $\beta_{\min} \le \beta_{com} \le \beta_{\max}$. Typical limits for short-range tactical platforms are $\alpha_{\max} \in [20°, 30°]$ and $\beta_{\max} \in [12°, 18°]$, noticeably wider than the $\alpha_{\max} = 10^\circ$ budget that shows up in hypersonic aeroballistic work [13]. This additional control authority is important because, in low-dynamic-pressure regimes, the angle of attack α becomes the primary means of generating and correcting the flight path. During operation, the guidance law must cope with four main sources of uncertainty: midcourse handover dispersion, wind and density variations, aerodynamic coefficient uncertainty (± 15% on ρC_y and ρC_z in our tests), and actuator tracking error.

2.4. Updatable hitting trajectory

Classical impact-angle control laws typically drive the approach angle to its desired value through feedback-based correction, which runs into trouble at steep dive angles $\Theta_f < -60^\circ$ where the required control easily saturates. We take a different route: at each update instant t_k the onboard computer reconstructs a new smooth reference trajectory $\{h_p(L), B_p(L)\}$ trajectory so that, in geometric terms, the aerial vehicle can approach the target with the exact angles prescribed at the design stage. Formally, at $L = L_f$:

$$h_p(L_f) = h_f, \quad B_p(L_f) = 0, \quad \left.\frac{dh_p}{dL}\right|_{L_f} = \tan\Theta_f, \quad \left.\frac{dB_p}{dL}\right|_{L_f} = \tan\Psi_f \tag{4}$$

and at $L = L(t_k)$ the trajectory matches the current estimated position and slopes: $h_p = \hat{h}(t_k)$, $B_p = \hat{B}(t_k)$, $\frac{dh_p}{dL} = \tan\hat{\Theta}(t_k)$, $\frac{dB_p}{dL} = \tan\hat{\Psi}(t_k)$. Between update instants, the aerial vehicle follows the current reference trajectory. At the next guidance cycle, the entire trajectory is reconstructed from the latest estimated state. This enables the closed-loop system to avoid excessive reliance on trajectory-error feedback, since the deviation is instead absorbed during the trajectory-reconstruction stage. At the same time, each newly generated reference trajectory is guaranteed to satisfy the terminal approach-angle constraint. Onboard the aerial vehicle, the algorithm is implemented in four consecutive steps. First, the state-estimation block provides the input data for trajectory reconstruction (Section 3.1). Next, the reconstructed trajectory is analyzed to determine the velocity components to be controlled. Then, the dynamic-inversion step for the

STT configuration (Section 3.2) converts these components into (α,β) control commands. Finally, command saturation limits are applied. With a guidance cycle Δt_g of 50 to 100 ms, the algorithm is well suited to common embedded processors and remains significantly faster than the approximately 0.3 s time constant of the autopilot system.

3. BEZIER TRAJECTORY GENERATION

3.1. Bezier curves as trajectory generators

A Bezier curve of degree n is built from $n+1$ control points $P_0, P_1, ..., P_n$ as $B(u)=\sum_{i=0}^{n} P_i \cdot C(n,i)\cdot u^i \cdot (1-u)^{n-i}$, $u\in[0,1]$. Two characteristics make this family of curves particularly suitable for the problem under consideration. First, the curve passes exactly through the initial P_0 and terminal P_n points, which makes it straightforward to satisfy the positional boundary conditions. Second, the tangent at each endpoint is always parallel to the segment connecting that endpoint to the adjacent control point, thereby allowing the angular boundary conditions to be imposed directly.

For the longitudinal channel we use coordinates $(L(u),h(u))$. The aerial vehicle's current state fixes (L_0,h_0,Θ_0) at $u=0$, and the aimpoint fixes (L_f,h_f,Θ_f) at $u=1$. A second-order Bezier has a single interior control point which, from the tangent condition, sits at the intersection of the two boundary tangent lines:

$$L_1=\frac{(h_0-L_0\tan\Theta_0)-(h_f-L_f\tan\Theta_f)}{\tan\Theta_f-\tan\Theta_0},\qquad h_1=h_f+(L_1-L_f)\tan\Theta_f \tag{5}$$

A third-order Bezier has two interior points; we place them along the boundary tangent lines at fractional distances $k_1,k_2\in(0,1)$ of the overall range, giving $h_1=h_0+|L_f-L_0|\cdot k_1\cdot\tan\Theta_0$ and $h_2=h_f+|L_f-L_0|\cdot k_2\cdot\tan\Theta_f$. The parameters k_1,k_2 control how the curvature is distributed along the trajectory; a symmetric default $k_1=k_2=1/3$ proves effective across the SRAV envelope. The lateral channel is built the same way, replacing h by B and Θ by Ψ.

3.2. Commanded body rates

Given the chosen curve, the slopes $h'_L=\frac{dh}{dL}$ and $h''_L=\frac{d^2h}{dL^2}$ at the current L follow by implicit differentiation: $h'_L=\frac{h'_u}{L'_u}$ and $h''_L=\frac{h''_u\cdot L'_u-h'_u\cdot L''_u}{(L'_u)^3}$, where h'_u, L'_u and h''_u, L''_u are the first and second derivatives of (5) with respect to u (straightforward closed-form expressions; omitted for brevity). The commanded flight path angle rate is then

$$\dot\Theta_{com}=\frac{h''_L}{1+(h'_L)^2}\cdot V\cos\Theta\cos\Psi \tag{6}$$

with the factor $V\cos\Theta\cos\Psi=\frac{dL}{dt}$ converting the spatial second derivative into a temporal rate. The lateral channel gives $\dot\Psi_{com}$ by the same derivation.

3.3. Inverse dynamics for STT

The guidance layer delivers commanded rates $\left(\dot{\Theta}_{com}, \dot{\Psi}_{com}\right)$; the inverse-dynamics layer converts them into $\left(\alpha_{com}, \beta_{com}\right)$. Solving (2) for the aerodynamic forces required to produce the commanded rates, with $\gamma \approx 0$, gives $Y_{com} = mV\left(\dot{\Theta}_{com} + \frac{g}{V}\cos\Theta\right)$ and $Z_{com} = -mV\cos\Theta \cdot \dot{\Psi}_{com}$. Linearizing the forces around the operating point, $Y \approx \frac{1}{2}\hat{\rho}V^2 S\left(\hat{C}_y^0 + \hat{C}_y^\alpha \alpha\right)$ and $Z \approx \frac{1}{2}\hat{\rho}V^2 S \cdot \hat{C}_z^\beta \beta$, and equating with the required values yields the closed-form commands

$$\alpha_{com} = \frac{1}{\hat{C}_y^\alpha}\left(\frac{2Y_{com}}{\hat{\rho}V^2 S} - \hat{C}_y^0\right), \qquad \beta_{com} = \frac{2Z_{com}}{\hat{\rho}V^2 S \cdot \hat{C}_z^\beta} \tag{7}$$

which, after substituting Y_{com}, Z_{com} and (6), depend only on the current state and on the Bezier derivatives at the current longitudinal coordinate. It should be emphasized that (7) is evaluated with the nominal parameters $\hat{\rho}$, $\hat{C}_y^\alpha$ and $\hat{C}_z^\beta$, independently of the true values governing the SRAV. The plant model is propagated using the true values ρ, C_y^α, and C_z^β, drawn randomly in each Monte Carlo trial (±15% for the aerodynamic derivatives and ±10% for density). The discrepancies $\rho - \hat{\rho}$ and $C_i - \hat{C}_i$ therefore constitute genuine uncertainty from the controller's viewpoint.

The raw commands are then passed through the saturation block $\alpha_{com} = \text{sign}\left(\alpha_{com}\right) \cdot \alpha_{\max}$ when they exceed the limit, and likewise for β. Because the guidance law contains no integral state persisting across cycles, integrator windup cannot arise structurally. When the command saturates, the following guidance cycle rebuilds the reference trajectory from the realized state, producing a reference-governor-like behavior in which the error degrades gracefully instead of accumulating.

4. SIMULATION RESULTS

4.1. Setup

Table lists the reference SRAV parameters, chosen to represent a small tactical class in the 20–30 km range bracket, typified by fielded systems such as the Spike-NLOS. The aerodynamic database was built from published correlations for this size class and trimmed for the STT assumption.

Table 1. *Reference SRAV parameters.*

Parameter	Unit	Value
Vehicle mass, m	kg	60
Reference area, S	m²	0.042
Lift stability derivative, C_y^α	rad⁻¹	4.5
Side-force stability derivative, C_z^β	rad⁻¹	−3.8
Max angle of attack, $\alpha_{\max}$	deg	30
Max sideslip, $\beta_{\max}$	deg	15
Autopilot time constant, $T_\alpha = T_\beta$	s	0.12
Guidance update period, Δt_g	ms	50

The nominal handover state is $h_0 = 800$ m, $V_0 = 380$ m/s, $L_f - L_0 = 4$ km, $B_0 = 0$, $\Theta_0 = -2°$, $\Psi_0 = 0°$; the aimpoint sits at $h_f = 5$ m (sea-surface engagement). The terminal phase begins when

the seeker acquires the target, typically at 3–5 km for laser or imaging-infrared seekers of this class, which is consistent with the 20–30 km total engagement range reached through a preceding midcourse phase under inertial and waypoint guidance. We examine two terminal approach angles: a shallow sea-skimming case $\Theta_f = -30^\circ$ and a steep dive $\Theta_f = -70°$, both with $\Psi_f = 0°$. Wind follows an ISA profile with 10 m/s sustained component and 3 m/s gusts, representative of typical maritime conditions at low altitude. The simulation runs at 1 kHz with fourth-order Runge-Kutta; the guidance law updates at 20 Hz, giving roughly 210 cycles over the ~10.5 s terminal phase.

4.2. Nominal trajectories

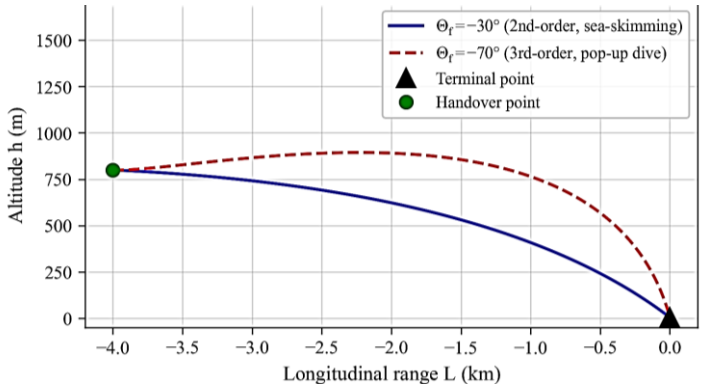


Figure 1. *Nominal trajectories in the longitudinal plane.*

Figure 1 shows the nominal trajectories for both scenarios. The hybrid strategy picks the second-order Bezier for the −30° case and the third-order for the −70° case. Both reach the aimpoint with less than 0.5 m in position error and 0.3° in flight path angle error. Figure 2 traces the control commands: α_{com} stays well within $\pm\alpha_{\max}$ and β_{com} within $\pm\beta_{\max}$ throughout. The steep-dive α profile is smooth and monotonic, in contrast to the discontinuous profiles that a classical-spline scheme produces for the same boundary conditions [13].

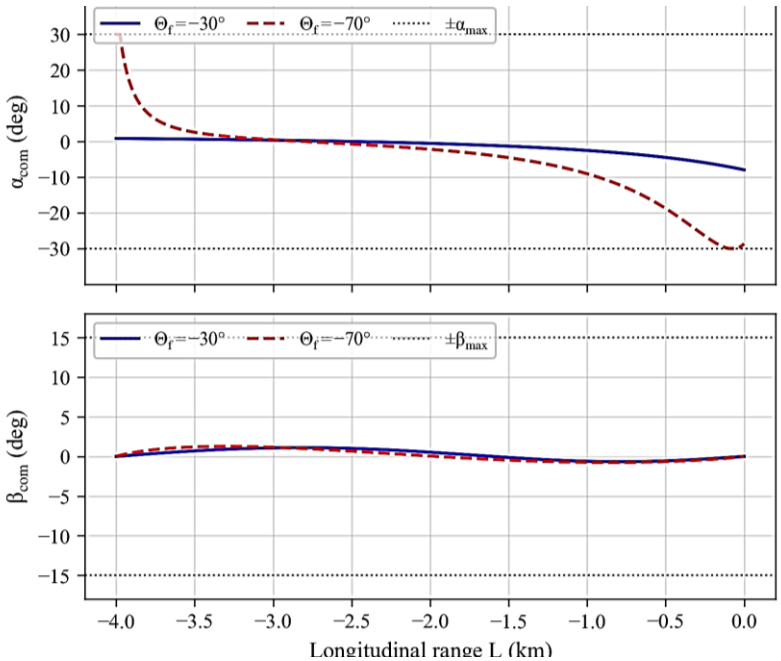


Figure 2. *Commanded α and β histories; saturation limits shown as dashed lines.*

4.3. Monte Carlo robustness

We ran 1000 trials per scenario, drawing each initial-state perturbation from a uniform distribution: $\Delta B_0 = \pm 50$ m, $\Delta H_0 = \pm 100$ m, $\Delta V_0 = \pm 15$ m/s, $\Delta\Theta_0 = \pm 1.0°$, $\Delta\Psi = \pm 1.0°$. Wind direction was randomized on each trial. Figure 3(a,b) shows the terminal impact dispersion for both scenarios; the CEP works out to 0.36 m for $\Theta_f = -30°$ and 0.48 m for $\Theta_f = -70°$.

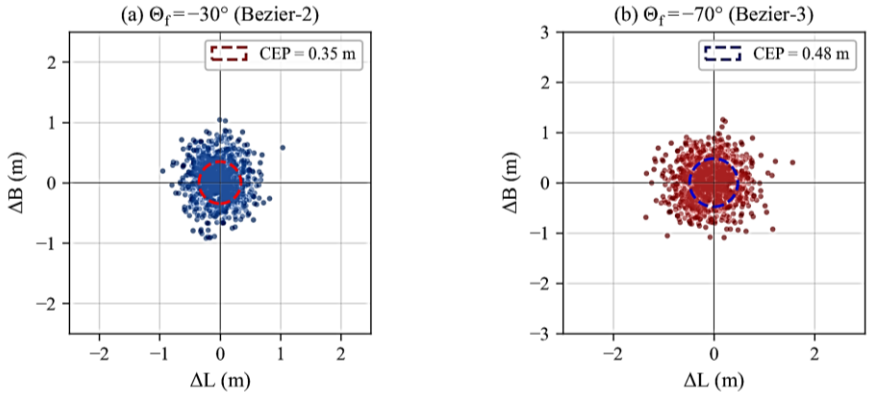


Figure 3. *Terminal impact dispersion (1000 Monte Carlo trials per scenario).*

4.4. Comparison with a biased proportional navigation baseline

For comparison with a classical guidance law, the same Monte Carlo campaign was conducted using Biased Proportional Navigation (BPN), with the commanded acceleration:

$$a_c = NV_c\dot{\lambda} + N_b\left(\lambda - \lambda_f\right), \text{ with } N = 4 \text{ and } N_b = 2.$$

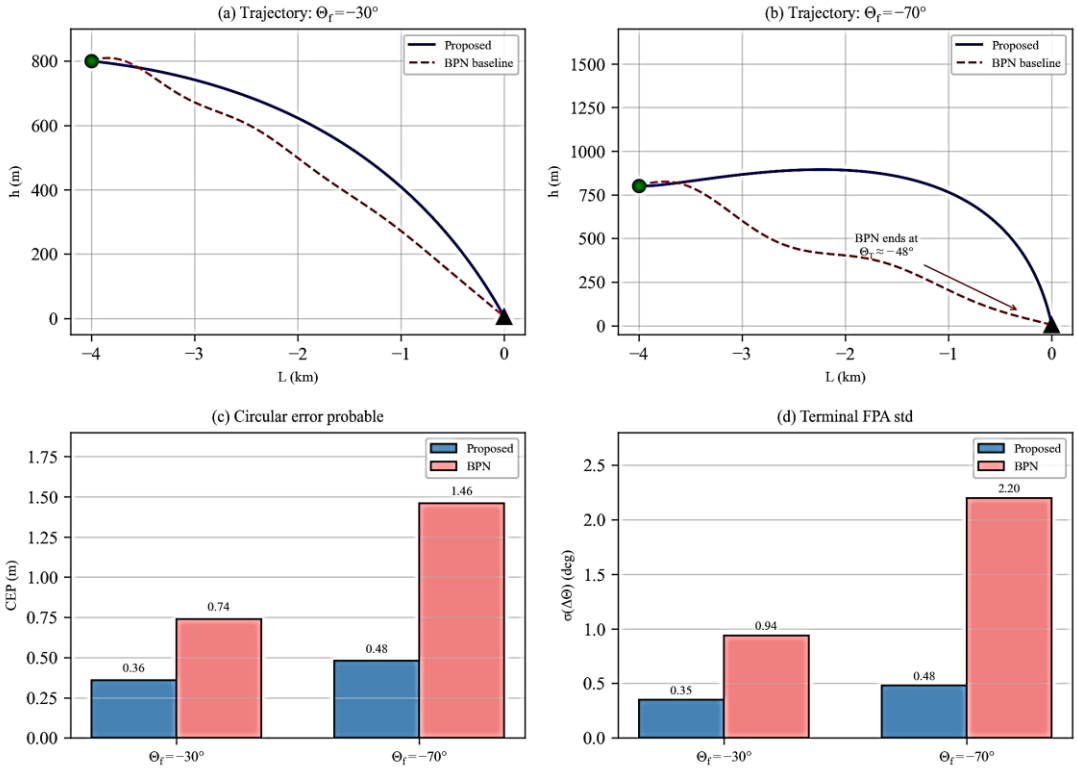


Figure 4. *Proposed vs BPN baseline — trajectories (a, b) and Monte Carlo metrics (c, d).*

The comparison results are shown in Figure 4. For the moderate approach-angle requirement of $\Theta_f = -30^\circ$ (Figure 4a), both methods successfully intercept the target with small impact-angle errors. However, the BPN trajectory still exhibits noticeable oscillations caused by the bias term, resulting in a larger impact-angle error of approximately 3°. When the required approach angle is increased to $\Theta_f = -70^\circ$ (Figure 4b), the limitations of BPN become evident. The guidance law can no longer generate sufficient maneuvering capability to achieve the prescribed impact angle while maintaining accurate target interception, yielding a final impact angle of only about - 48°. In contrast, the proposed guidance law generates a climb-and-dive trajectory by continuously reconstructing a third-order Bézier reference trajectory at each guidance cycle.

The quantitative results further demonstrate the superiority of the proposed method. For $\Theta_f = -30^\circ$, it achieves a CEP of 0.36 m and an impact-angle-error standard deviation of only 0.35°, compared with 0.74 m and 0.94°, respectively, for BPN. When $\Theta_f = -70^\circ$, the CEP increases only slightly to 0.48 m, whereas BPN reaches 1.46 m. Likewise, the standard deviation of the impact-angle error is reduced from 2.20° to 0.48°. Moreover, the angle-of-attack command reaches saturation in fewer than 5% of the Monte Carlo runs, compared with more than 25% for BPN, indicating that the proposed guidance law utilizes the available control authority more efficiently while maintaining high accuracy even under demanding steep-impact-angle conditions.

5. CONCLUSIONS

The terminal guidance law presented here takes a fairly direct route to the simultaneous requirements of submeter accuracy and prescribed impact angle for short-range STT vehicles. Rebuilding a smooth Bezier hitting trajectory at each guidance cycle, and mapping the resulting commanded body rates to (α, β) commands in closed form, gives a scheme whose computational cost is a small multiple of a PN update while its terminal performance is competitive with optimal formulations. The hybrid between second- and third-order Bezier covers the tactical envelope from shallow sea-skimming to near-vertical dive, and the Monte Carlo results confirm sub-meter CEP and below -1.5° angular accuracy under realistic handover, wind, and aerodynamic dispersion.

The present work assumes a stationary aimpoint and models the seeker only through its effect on the regeneration-cycle initial condition. Three natural extensions suggest themselves: coupling the regeneration step with an extended Kalman filter so the state estimate tolerates noisier and intermittent seeker returns; letting the aimpoint move, which amounts to rebuilding the reference against a predicted terminal position; and a hardware-in-the-loop campaign on a representative ARM Cortex-M7 platform to pin down the update rate achievable alongside the navigation and autopilot workloads.

REFERENCES

[1]. P. Zarchan, "*Tactical and Strategic Missile Guidance*", 6th ed., AIAA, Reston, VA, USA, (2012).
[2]. N. A. Shneydor, "*Missile Guidance and Pursuit: Kinematics, Dynamics and Control*", Horwood, Chichester, U.K., (1998).
[3]. S. Chen, W. Wang, J. Fan et al., "*Impact angle constraint guidance law using fully-actuated system approach*", Aerospace Science and Technology, Vol. 136, p. 108220, (2023).
[4]. X. Kong, C. Zhang and F. Xiong, "*Impact speed and angle constrained guidance law for unpowered gliding vehicle*", Chinese Journal of Aeronautics, Vol. 38, No. 4, (2025).
[5]. Y. Li, J. Liu, J. Shan and J. Wang, "*Guidance law with terminal velocity constraint for hypersonic morphing vehicle*", Advances in Guidance, Navigation and Control (ICGNC 2024), Springer, Singapore, (2025).
[6]. A. Li, X. Hu, S. Yang and K. Dong, "*Adaptive terminal time and impact angle constraint cooperative guidance strategy for multiple vehicles*", Drones, Vol. 8, No. 4, p. 134, (2024).

[7]. Y. He, F. Guo, H. Zhang and S. Chen, "*Pre-defined time convergent non-singular terminal sliding mode guidance law with impact angle constraint*", Proceedings of the Institution of Mechanical Engineers, Part G: Journal of Aerospace Engineering, (2025).
[8]. Z. Hu, W. Yi and L. Xiao, "*Deep reinforcement learning-based impact angle-constrained adaptive guidance law*", Mathematics, Vol. 13, No. 6, p. 987, (2025).
[9]. L. Liang, B. Zhao, J. Zhou and Z. Zhang, "*Impact angle controlled integrated guidance and control with input and state constraints*", International Journal of Control, Vol. 97, No. 4, pp. 796–810, (2024).
[10]. J. Guo, Y. Zhou and M. Zhou, "*Adaptive control law based integrated guidance and control design for missile with the radome error compensation*", Proceedings of the Institution of Mechanical Engineers, Part G: Journal of Aerospace Engineering, Vol. 238, No. 4, pp. 361–371, (2024).
[11]. P. Kumar, G. Joseph, C. R. Murthy and R. Padhi, "*Comprehensive MPSP for fast optimal control: Algorithm development and convergence analysis*", Transactions of the Indian National Academy of Engineering, Vol. 10, pp. 33–52, (2025).
[12]. Y.-Z. Wang and H.-H. Dai, "*Secure model predictive static programming with initial value generator for online computational guidance of near-space vehicles*", Aerospace Science and Technology, Vol. 156, p. 109768, (2025).
[13]. H. Shi, Z. Cheng, M. Kuang, J. Zhu, X. Yan and X. Li, "*Four-stage guidance law for impact time and angle control based on the Bezier curve*", IEEE Transactions on Aerospace and Electronic Systems, Vol. 60, No. 4, pp. 3766–3778, (2024).
[14]. S. Coskun, A. Catak and E. Koyuncu, "*3D impact time and angle control based on Apollo guidance and Bezier curves*", Journal of Guidance, Control, and Dynamics, (2025).
[15]. W. Chen, P. Sui, Y. Qian et al., "*Cubic Bézier shaping impact angle constrained guidance for intercepting maneuvering targets*", Nonlinear Dynamics, Vol. 114, No. 3, Art. No. 192, (2026). DOI: 10.1007/s11071-025-12057-4.

TÓM TẮT

Giải pháp nâng cao luật dẫn đường pha cuối cho thiết bị bay tầm ngắn trong điều kiện ràng buộc góc va chạm và bất định khí động học

Trong bài toán dẫn đường pha cuối cho thiết bị bay tầm ngắn, đặc biệt với các kịch bản tiếp cận mục tiêu trên biển, việc đảm bảo góc tiếp cận yêu cầu là yếu tố quyết định để phát huy hiệu quả của nhiệm vụ. Cùng một thiết bị bay, nếu tiếp cận mục tiêu với góc phù hợp sẽ cho hiệu quả cao hơn rõ rệt so với trường hợp chỉ bảo đảm đúng vị trí nhưng không thỏa mãn góc tiếp cận tối ưu. Tuy nhiên, yêu cầu này rất khó thực hiện trong thực tế do ảnh hưởng đồng thời của gió biển biến đổi liên tục và các bất định khí động học khi phương tiện bay làm việc ở vùng áp suất động thấp gần mặt biển.. Bài báo này đề xuất một luật dẫn đường pha cuối cho thiết bị bay tầm ngắn dạng điều khiển trượt-quay, trong đó quỹ đạo tiếp cận được tái sinh tại mỗi chu kỳ dẫn đường dưới dạng đường cong Bezier bậc hai hoặc bậc ba, đảm bảo đồng thời điều kiện vị trí và góc tại điểm tiếp cận. Từ quỹ đạo tham chiếu này, các tốc độ góc yêu cầu được chuyển đổi thành lệnh điều khiển góc tấn công α và góc trượt cạnh β thông qua một bước nghịch đảo động lực học ở dạng giải tích khép kín. Kết quả mô phỏng Monte Carlo trên mô hình tham chiếu cho thấy phương pháp đề xuất đạt sai số vòng tròn xác suất dưới 1 m và sai lệch góc đường bay cuối nhỏ hơn 1.5°, đồng thời duy trì được tính ổn định trước các bất định của gió, mật độ khí quyển và hệ số khí động học.

Từ khoá: Bất định khí động học; Đường cong Bézier; Góc va chạm; Dẫn đường trên khoang; Dẫn đường pha cuối; Tái tạo quỹ đạo.